Wave-Based Simulation of Wind Instrument Resonators

Maarten van Walstijn

Sonic Arts Research Centre, School of Electronics, Electrical Engineering, and Computer Science
Queen's University Belfast, UK.

1 Introduction

Time-domain modeling of musical instruments has been an active area of study for a few decades now. The objective for developing such predictive models is generally twofold. Right from the first developments [1, 2, 3], a major aim has been to create a better understanding of how sound is generated with instruments, providing insights and results that cannot be obtained within a frequency-domain approach due to the non-linearities involved. While some early models were already used for generating audio output examples [4], the potential for musical sound synthesis applications has only become significant with the steady increase of commonly available digital processing power. The two objectives (i.e. 'understanding' and 'physics-based synthesis') cannot really be seen as independent; they can be said to 'converge' with model precision, i.e. good time-domain model should also sound realistic. Generally, computational efficiency tends to be a higher priority when the main objective is sound synthesis, especially if a real-time implementation is required. In comparison with classical, waveform-oriented sound synthesis methods, such as additive synthesis or FM synthesis, the physical modeling approach offers the crucial advantage of inherent simulation of natural transients, and in addition provides a direct link between model parameters and the real-life actions of a player.

The first wind instrument time-domain simulation to appear in the literature is the clarinet model by Schumacher [2]. In this model, the response of the instrument air column is computed by means of a convolution with its impulse response. The convolution is part of a non-linear feedback loop that forms the basic structure of a physical model of a wind instrument (see Figure 1), where the non-linear part corresponds to the reed excitation mechanism. This type of formulation was later generalized for simulation of a wide variety of self-sustaining musical oscillators by McIntyre, Schumacher and Woodhouse [3], and has since been adopted and developed further by a large number of researchers (see for example, [5, 6]). Although remarkably realistic

sound output can be obtained within this approach, the convolution method is not particularly convenient for application to musical sound synthesis due to the fact that a different impulse response is required for each configuration of the instrument bore. For example, in order to simulate the functioning of the valves of a trumpet, the model would have to switch or interpolate between a large set of impulse responses. In order to enable precise control of those parts of the instrument that are used for pitch adjustment (i.e., toneholes, valves, or slides) without having to resort to methods which require large amounts of computational power and storage space, a *spatially modular* approach is required. That is, if the instrument is modelled as a series of interacting modules, these modules can be controlled independently, which tends to allow for a much more direct, simpler and musically more meaningful form of parameterization. For example, a modular clarinet model consists of a series of cylindrical bore sections and tonehole units, and in a way analogous to a real clarinet player, the pitch of the instrument can then be adjusted by opening and closing of the holes.

This paper focuses on modular, wave-based discrete-time modeling of the resonator oscillations. The main advantage of using a wave-based approach is that it explicitly simulates the way in which waves build up in a real instrument, and therefore inherently yields a spatial representation. The wave-based approach also happens to be computationally efficient, mainly due to the fact that lossless traveling of waves in 1D waveguides can be implemented with very few arithmetic operations. With regard to modeling the excitation mechanism, we refer to the literature, that provides general overviews (e.g. [7, 8, 9]), as well as many instrument-specific models (e.g. [10, 11, 12]).

The paper is organized as follows. The main concepts and methods for wave-based modeling of wind instrument bores, are explained in Section 2. Section 3 explains wave digital modeling of piecewise conical section in more detail, and section 4 describes a full wave digital model of the trumpet. Finally some concluding remarks and suggestions for future research are outlined in Section 5.

2 Modular Approaches to Wave-Based Modeling

2.1 Digital Waveguide Modeling

The digital waveguide modeling (DWM) approach is based on spatial-temporal sampling of the traveling-wave solutions of 1D waveguides [13], and is therefore particularly suited to modeling wave propagation in non-flaring ducts (i.e. cylindrical and conical duct sections). For example, lossless pressure oscillation in a cylindrical duct is described by the equation

$$\frac{\partial^2 p}{\partial x^2} = \frac{1}{c^2}\frac{\partial^2 p}{\partial t^2}, \tag{1}$$

where p denotes pressure as a function of position (x) and time (t). It is well-known that the solutions of Equation 1 can be written as a sum of two pressure waves traveling in opposite directions, with speed c. At

any point $x = x_i$ in a duct of cross-section S, these waves (p_i^+, p_i^-) are related to the local pressure p_i and volume velocity u_i by

$$p_i = p_i^+ + p_i^- \quad \text{and} \quad u_i = \frac{p_i^+ - p_i^-}{Z_0}, \tag{2}$$

where $Z_0 = \rho c/S$ is the characteristic impedance, and ρ is the mean air density. Considering then a cylindrical duct section of length L (see Figure 2(a)), the relationship between the Fourier transforms of the pressure waves at either side of the section may be written expressed by the transfer function

$$H(\omega) = \frac{P_2^+}{P_1^+} = \frac{P_1^-}{P_2^-} = e^{-jkL}, \tag{3}$$

where $k = \omega/c$ is the wave number, and where ω denotes angular frequency. In the case of neglecting the effects of wall losses, $H(\omega)$ is merely the frequency-domain representation of a delay of L/c seconds. This can be simulated in discrete-time as follows. Given a sample period $T = 1/f_s$, wave propagation from one end to the other is simulated with a delay-line of integer length N in series with a fractional delay filter that implements a non-integer delay-length of D samples; the total delay $(N + D)T$ realized by this series should closely approximate L/c within the lower part of the frequency range. Wave propagation occurs in two directions, and the pressure at a specific point along the duct axis can be found by summing the forward- and the backward-traveling waves at that point. For realizing a fractional delay, various types of filters designs can be applied, amongst which lower-order Thiran all-pass filters and Lagrange FIR interpolation filters are most commonly used [14].

Accurate modeling of a cylindrical bore however requires incorporating the effects of viscothermal wall losses; not doing so would lead to incorrect amplitudes and frequencies of the natural resonances of the simulated instrument. Viscothermal losses can be taken into account by re-writing the transfer function as:

$$H_L(\omega) = e^{-\Gamma L}, \tag{4}$$

where Γ is a lossy, complex-valued propagation constant [7]. The lossy transfer function $H_L(\omega)$ contains the same delay-term as the lossless transfer function. As in the lossless case, this delay can be simulated by means of a delay-line. What remains is to model the propagation losses, which can be formulated with the transfer function:

$$H_{loss}(\omega) = \frac{H_L(\omega)}{H(\omega)} = \frac{e^{-\Gamma\, L}}{e^{-j\,\omega\, L/c}}. \tag{5}$$

We can approximate this expression with a digital filter, and implement the complete propagation path by cascading this "loss-filter" with the delay-line. The resulting lossy digital waveguide structure is depicted in Figure 2(b). The most straightforward way to approximate the propagation losses is by means of an FIR filter

[15]. However, for obtaining accurate results the FIR filter needs to be very long and therefore expensive. Designing accurate lower-order IIR designs has been shown to be possible, using well-known methods such as Prony, Hankel and output-error designs [16, 17]. The main drawbacks of these techniques are (1) their complexity involved in computing the filter coefficients and (2) the lack of robustness with variation of the duct parameters [16]. This makes these techniques unsuitable, for example, for application to modeling a trombone slide, which requires dynamic variation of the filter. Abel et al. [17] developed a robust, parametric IIR design, using cascaded first-order shelving filters, which gives very accurate results (deviation within a fraction of a dB) for the entire audio bandwidth for filter orders as low as 4. The only small drawback of their approach is, since the design is an ad-hoc fit, it does not converge towards the ideal response with increasing filter order.

Frequency-dependent termination losses, such as occur at the open end of a duct, are simulated using a digital filter that is designed to approximate the termination reflectance

$$R_L(\omega) = \frac{Z_L(\omega) - Z_0}{Z_L(\omega) + Z_0}, \tag{6}$$

where $Z_L(\omega)$ is the termination load. For most wind instruments, the radiation impedance of unflanged open ends as formulated by Levine and Schwinger [18] gives a suitable formulation of the termination load. Scavone [19] gives a convenient wide-band approximation to these formulas. For discrete-time modeling of an open-ended cylindrical duct, a reflectance filter $R_L(z)$ has to be inserted into the structure in Figure 2(b) such that it calculates the backward-traveling wave p_2^- from forward-traveling wave p_2^+.

• *Conical Sections*

The main bore of many wind instruments, such as the saxophone or the bassoon, is not cylindrical but conical. As with the cylindrical duct, the solution to the conical duct wave equation can be written as a sum of a forward- and a backward- traveling wave [7]. One essential difference is that the pressure waves are now scaled by the distance r from the cone apex. Hence propagation of spherical pressure waves inside a conical section can be modelled in the same way as for cylindrical section, using a cascade of a delay-line, a fractional delay filter and a loss-filter, but with an added scaling term to account for the spreading of the wavefront over a varying cross-section. A second difference in comparison with a cylindrical section is that the characteristic impedance is now frequency-dependent [7]. The main consequence is with regard to formulating scattering junctions between sections. It was shown in [16] that a general junction model, that models a junction between any two non-flaring sections (see for example the junction between two conical section Figure 3(a)), can be formulated as depicted schematically in Figure 3(b), where for a given where wavefront ratio $B = S_2/S_1 = (a_2/a_1)^2$, the

	IIM	TICM	BT
b_0	$\left(-1+e^{\alpha T}\right)$	$-1-\frac{e^{-\alpha T}-1}{\alpha T}$	$\frac{\alpha}{\alpha+\beta}$
b_1	0	$e^{-\alpha T}+\frac{e^{-\alpha T}-1}{\alpha T}$	$\frac{\alpha}{\alpha+\beta}$
a_1	$e^{-\alpha T}$	$e^{-\alpha T}$	$\frac{\alpha-\beta}{\alpha+\beta}$

Table 1: Coefficients of the digital junction filter. $\beta = 2/T$ is the bilinear operator.

coefficients are

$$C_1 = \frac{2B}{B+1}, \quad C_2 = \frac{2}{B+1}, \quad C_3 = \frac{B-1}{B+1}, \tag{7}$$

and where the element $R_j(z)$ is a digital approximation to the analog junction filter:

$$R_j(s) = \frac{-\alpha}{s+\alpha}, \quad \text{with} \quad \alpha = \frac{\gamma_2 S_2 - \gamma_1 S_1}{S_2 + S_1}, \tag{8}$$

where $\gamma_1 = c/r_1$ and $\gamma_2 = c/r_2$. For a cylindrical section, we have $\gamma = 0$. Hence if both sections are cylindrical, α equals zero, and the junction filter becomes inactive, not passing through any signal, and the structure in Figure 3(b) 'collapses' into a standard "Kelly-Lochbaum junction" that implements a wavefront surface discontinuity.

Various different methods can be used to discretize the analog junction reflection filter. Välimäki [20] applied the impulse invariance method (IIM), whereas Scavone [19] and Amir [21] obtain a discrete-time version of the junction filter via the bilinear transform. A third method can be found in the work by Martínez et al. [22], who obtain the reflected wave by means of a recursive formulation of time-interpolated convolution of the junction filter impulse response with the incident pressure wave. We will refer to this method as the "time-interpolated convolution method" (TICM). It can easily be shown that all three methods are equivalent to passing the incident pressure wave through a first-order digital filter:

$$R_j(z) = \frac{b_0 + b_1 z^{-1}}{1 + a_1 z^{-1}}. \tag{9}$$

Table 1 summarizes the coefficients as derived with these methods. For all three, the digital junction filter is exact at DC, and exhibits an increase in the deviation from the ideal filter with frequency. The responses obtained with the TICM and the BT are usually extremely similar, except for extreme values of α that correspond to modeling extreme taper discontinuities.

All three discretization methods mentioned above convert stable analog filters into stable digital filters. Hence if the analog junction filter $R_j(s)$ is stable, then its discrete-time counterpart $R_j(z)$ is also stable. Unfortunately, $R_j(s)$ is not stable for all physically feasible cases [20, 19]. From Equation 8 we can see that

the analog filter is only stable if $\alpha > 0$. This is true if

$$\frac{1}{r_2} > \frac{B}{r_1}. \tag{10}$$

The use of an unstable filter element is generally seen as problematic, since its impulse response exhibits unstable growth. However, the continuous-time model of a bore with conical sections has been shown to be stable despite the existence of local unstable elements [23, 24]. Although no proof has been found, numerous tests with conical bore systems have indicated that the discrete-time model also remains stable under certain circumstances. That is, no evidence of unstable growth have been found whenever (1) using the bilinear transform or the TICM to discretize the junction filter, and (2) not including any loss-filters in the conical sections of the bore model. Instability due to round-off errors only appears to take hold in implementations where low number precision is used. However, including losses in conical sections generally causes instability problems [16], and therefore specific solutions are required to implement such models (see Section 3.3).

2.2 Wave Digital Modeling

Wave digital modeling (WDM) is a technique that combines DWM with wave digital filter (WDF) techniques [25]. The latter were designed for discretization of analog networks [26]. The resulting digital networks are called *wave digital filters* (WDFs). The classical analogy between electric and acoustic systems raises the possibility of employing WDF techniques for the discretization of lumped elements in a model of an acoustic system. WDF techniques are similar to DWM techniques in the sense that they both digitize continuous-time models using wave variables. This section summarizes the modeling principles of this approach with respect to time-domain modeling of wind instrument bores.

Wave digital models are derived from a transmission-line description of a wind instrument bore. The approach thus requires that a transmission-line description or "equivalent network" is found for each individual bore component. The procedure for the derivation of the wave digital model of an individual bore component is similar to the derivation of a wave digital filter, and consists of three steps:

(1) decomposition of the acoustic (Kirchhoff) variables into wave variables.

(2) discretization of frequency-dependent elements.

(3) satisfaction of the computability condition.

Step (1) is accomplished by using the following relationships:

$$p_i = p_i^+ + p_i^- \quad \text{and} \quad u_i = \frac{p_i^+ - p_i^-}{R_i}, \tag{11}$$

where for port i, p_i is the pressure and u_i is the volume velocity, while p_i^+ and p_i^- are the wave variables. The quantity R_i has the dimension of resistance and, following WDF theory, is referred to as the *port-resistance*. In the case of simulating a distributed acoustic element (such as a cylindrical or conical section), the port-resistance is set equal to the local characteristic impedance, and the wave variables represent actual pressure waves traveling through a duct. The formulation is then exactly the same as with digital waveguide modeling (see Equation 2). In the case of a lumped acoustic element, the wave variables do not represent waves that actually travel any distance; the decomposition is in this case merely a matter of mathematical description, and from an acoustical point of view the port-resistance may then be considered arbitrary. As in the derivation of WDFs, this freedom of choice is exploited to avoid delay-free loops in the final modeling structure. The decomposition of acoustic variables has to be carried out at each port of the system. Figure 4 depicts a single port (a) and its corresponding signal flow after decomposition (b).

Step (2) concerns the approximation in the digital domain of linear, frequency-dependent, continuous domain phenomena, by means of digital filters. One category of these comprise lumped elements, such as inertances and compliances, which are mathematically described by a rational polynomial transfer function of the Laplace variable s. As is customary in WDF theory, such elements are discretized via the bilinear transform (BT):

$$s = \frac{2}{T}\left(\frac{1 - z^{-1}}{1 + z^{-1}}\right), \tag{12}$$

Other frequency-dependent phenomena, including viscothermal losses, fractional delays, and open-end reflectances, are treated in the same way as with DWM. Due to the frequency warping effect caused by the BT, wave digital models are accurate only at the lower frequencies. This works well for modeling wind instruments, because the internal bore oscillations are always dominated by low-frequency components.

Step (3) is concerned with the computability of the resulting digital structure. Like a digital filter, a wave digital model is described mathematically by a system of difference equations. Such a system is called *computable* if the arithmetic operations prescribed by these equations can be ordered sequentially at each discrete-time instant [26]. In practice this condition is satisfied if the system contains no delay-free loops. In a wave digital model, such delay-free loops may arise in the discretization of a lumped element. One possible way to solve this problem is to insert a fictitious delay into the loop. However, such an approach leads to significant errors, unless a very high sample rate is used. Following WDF theory, these loops can be ensured to have at least one delay by choosing the appropriate port-resistance of that loop. For example, consider the loop in Figure 4(c), in which $H(z)$ represents the digital transfer function of the loop. In a wave digital model, this transfer function can always be written in the form:

$$H(z) = \frac{b_0 + b_1\, z^{-1} + \ldots + b_N\, z^{-N}}{1 + a_1\, z^{-1} + \ldots + a_N\, z^{-N}}, \tag{13}$$

where the coefficients b_k, a_k depend on the port-resistance of the loop. The coefficient b_0 represents the *instantaneous reflection*. Hence in order for this loop to be computable, this factor must be zero. If $H(z)$ represents a lumped element, the port-resistance must then be chosen such that $b_0 = 0$.

2.3 Related Approaches

• *The Multiconvolution Approach*

Some decades ago, Martínez et al. [22] developed methods for time-domain modeling of woodwind bores. In their original "multiconvolution algorithm", the spacing between discontinuities is constrained to be a multiple of the spatial sampling interval. This limitation was later removed by Barjau et al. [27]. There are strong similarities between the wave digital modeling approach and the multiconvolution approach. Firstly, the approaches employ the same modeling framework. That is, the response of a woodwind bore is computed by explicitly simulating the transmission and reflection of pressure waves in the bore. Secondly, many of the typical bore discontinuities (such as toneholes and taper changes) are based on equivalent continuous-time models.

The main difference with the WDM method is the way in which frequency-dependent elements are discretized. The junction filter is modelled in discrete-time using the time-interpolated convolution method (TICM), and viscothermal losses and fractional delays are modelled directly via convolution (the equivalent of using an FIR filter). Interestingly, the TICM effectively provides a method for designing FIR loss-filters for high-precision applications, giving excellent results especially if high sample rates and filter orders can be used. However it is not very suited to real-time simulation on standard processors, due to the high computational cost involved. A more detailed comparison between the multiconvolution approach and the WDM approach can be found in [16].

• *Ducasse's Method*

Ducasse [28] uses the same underlying transmission-line model of the bore. In discrete-time, each tubular element is represented by a two-port system calculated through its transmission and reflection functions. Because the input and output waves of each system are defined as plane-wave pressure waves, no unstable elements arise in any of the elements. However, this approach results into incomputable loops whenever a tapered section is coupled to a lumped element or another tapered section. To overcome this problem, Ducasse applies the same simplification as originally used by Schumacher [2] in the use of the reflection function method, which is to assume that the first element of any reflection function in the system equals zero. The main advantage of this method is that it is unconditionally stable. The main disadvantage is that it is inaccurate for certain tubular geometries, especially in cases where there is a significant discontinuity

in cross-section and/or taper, for which the effects of the assumption of a zero instantaneous reflection are not negligible. It is worth noting that this is the case in many wind instrument mouthpieces, and that very small perturbations near the air column entry can have very strong effects on the resonance properties of the instrument. It is also true though that the effect of the assumption decreases with sampling frequency, i.e. one can always choose the sample rate sufficiently high such that the effect of the simplification becomes negligible. In summary this method is computationally expensive, due to (1) the many large filters to be used, and (2) the need to choose high sample rates in order to achieve accuracy. It is therefore more suited to off-line applications than real-time synthesis.

3 Piecewise Conical Sections

A woodwind bore may be considered as a succession of conical and cylindrical bore sections with a set of open or closed holes in their sides [22]. Similarly, a brass instrument usually contains various conical and cylindrical sections. This section presents methods for simulation of piecewise conical bores with the WDM method.

3.1 Transmission-Line Model of a Conical Section

It is well known that a conical section may be formulated as a transmission-line model, consisting of a pair of inertances, a transformer, and a non-tapered duct [29]. This equivalent network is depicted in Figure 5. The values of the inertances are $M_0 = \rho r_0/S_0$, and $M_e = \rho r_e/S_e$, where r_0 and r_e are the distances from the cone apex and S_0 and S_e the wavefront areas at the left-hand and right-hand side of the cone, respectively. The distance from the cone apex is defined as negative if the apex is positioned on the right-hand side of the cone. The WDM method can be used to derive a digital simulation of the equivalent circuit; a shunt inertance is modelled as a three-port junction with a single delay attached to one of its ports, and a bi-directional delay-line simulates the uniform line, with added filters for time-interpolation and inclusion of viscothermal losses. The transformer represents the decrease in pressure with increasing wavefront area, and can be modelled by adding a scaling factor to each delay-line. However, these scaling factors may be removed from the system without changing the overall reflectance at the input-end of the model. In such a scenario, one must apply them "extrinsically" when calculating the actual pressure at any point in the cone [16].

3.2 Wave Digital Junctions

An equivalent network of two successive conical sections can be constructed by attaching two networks of the kind depicted in Figure 5. A junction of two conical sections is thus described with a network which has the right-hand inertance $M_1 = -(\rho r_1)/S_1$ of the first cone in parallel with the left-hand inertance $M_2 = (\rho r_2)/S_2$ of the second cone. As pointed out by Benade [29], this arrangement of the junction network is equivalent to

a single shunt inertance (see Figure 6a)

$$M_j = \frac{M_1\, M_2}{M_1 + M_2} = \frac{\rho\, r_1\, r_2}{r_1\, S_2 - r_2\, S_1}. \tag{14}$$

This is a three-port network to which Kirchhoff's laws apply, i.e. $p_1 = p_2 = p_3$ and $U_1 = U_2 + U_3$. The shunt inertance defines the Laplace-domain relationship $p_3 = sM_j\, U_3$. The first step in the derivation of the wave digital junction is to decompose all the Kirchhoff variables into wave variables, which yields the signal flow structure depicted in Figure 6b. The three-port scattering equations are

$$p_1^- = p_2^- + W, \quad p_2^+ = p_1^+ + W, \quad p_3^+ = p_1^+ + p_2^- - p_3^- + W, \tag{15}$$

where $W = k_1 \left[p_1^+ - p_3^-\right] + k_2 \left[p_2^- - p_3^-\right]$, with the coefficients

$$k_1 = \frac{R_2\, R_3 - R_1\, R_3 - R_1\, R_2}{R_2\, R_3 + R_1\, R_3 + R_1\, R_2}, \quad k_2 = \frac{R_1\, R_3 - R_2\, R_3 - R_1\, R_2}{R_2\, R_3 + R_1\, R_3 + R_1\, R_2}. \tag{16}$$

In the continuous domain, the waves p_3^+ and p_3^- are related through the frequency-dependent wave reflectance

$$R(s) = \frac{M_j s - R_3}{M_j s + R_3}. \tag{17}$$

Now applying the BT yields the digitized wave reflectance

$$R(z) = \frac{\alpha - z^{-1}}{1 - \alpha z^{-1}} \quad \text{with} \quad \alpha = \frac{\beta M - R_3}{\beta M + R_3}, \tag{18}$$

where $\beta = 2/T$ is the bilinear operator. In order to avoid an incomputable loop, we must set $R_3 = \beta M_j$, so that $\alpha = 0$ and $R(z) = -z^{-1}$. Hence p_3^- can be computed by simply negating the value of p_3^+ at the previous time instant. This model is mathematically equivalent to the digital waveguide junction depicted in Figure 3(b) when using the bilinear transform to discretize the junction filter. However this realization has the advantage of requiring only two multipliers, k_1 and k_2.

Now consider the network in Figure 7a. This network is the electrical equivalent of a conical section that is terminated by a load $Z_L(\omega)$. This load could for example represent the open-end radiation impedance. The value of the shunt inertance at the termination is $M_j = -(\rho r)/S$, where r is the distance from the cone apex to the end of the cone, and S is the wave area at the cone end. Figure 7b shows the wave digital model of this system. The term $R_L(z)$ indicates a digital filter approximation of the wave reflectance

$$R_L(\omega) = \frac{Z_L(\omega) - R_2}{Z_L(\omega) + R_2}, \tag{19}$$

where R_2 is the port-resistance as defined for the wave variables p_2^+ and p_2^-. If the taper junction modelled in discrete-time without taking special care concerning the wave reflectances (i.e. if R_2 is set equal to the local characteristic impedance), then the system would exhibit a delay-free loop, because in that scenario both the junction and the lumped element have a non-zero instantaneous reflection. In order to avoid such a delay-free loop, the junction near the lumped element is designed in such a way that it has no immediate reflection of the wave incident coming from the right. It will therefore be referred to as a "WD-r junction", where the letter r indicates that the junction has a zero instantaneous reflection in right-going direction. This is achieved by setting $R_2 = (R_1 R_3)/(R_1 + R_3)$, where R_1 equals the local (planar wave) characteristic impedance and $R_3 = \beta M_j$ is the port-resistance associated with the junction shunt inertance. Similarly, one may derive a "WD-l junction", that has a zero instantaneous reflection on its left side [16].

3.3 Stable Implementation using Switched Bore Instances

For a normal wave digital junction (inertance given by Equation 14), the inertance remains positive only if $S_2/r_2 > S_1/r_1$. Hence for certain, physically feasible junction configurations, the junction inertance M_j is negative. This amounts to using a negative port-resistance, which normally leads to an unstable filter structure [26]. The unstable regions are exactly those defined by Equation 10. As mentioned in Section 2.1, including viscothermal losses in conical sections leads to instability problems. Simulation tests with the WDM method indicate that although the simulation becomes unstable when loss-filters are inserted in the conical sections, the output can still be computed without significant side-effects for long simulation times [16]. Hence the output can generally be calculated for a length of the order of the impulse response, without suffering from the effects due to inherent instabilities. In practice we found that this may not always hold for very narrow conical sections with high losses, in which case the undesired effects of unstable growth within a certain finite time frame can be reduced to manageable proportions by reducing the amount of losses somewhat.

The computability of finite-length outputs longer than the effective impulse response allows a stable implementation that employs two instances of the same wave digital model of the bore, running in parallel. At any time, only one of the two instances is actively computing the output, while the other is merely 'warming up'. After a period of N samples, the active instance becomes inactive, and the inactive instance becomes active, i.e. they are 'switched'. At the moment of switching, the new inactive instance is 'reset'. That is, all its memory values are set to zero; this includes all filter memories as well as all delay-lines of the model. The switching period N has to be chosen larger than the effective length of the impulse response of the bore model (typically shorter than 1 second). This way the switching does not cause significant discontinuities in the output signal. The effective impulse response of the switched system is of finite length $2N$, and the system is guaranteed to be stable, thus making it suitable for application to musical sound synthesis.

4 Application to the Trumpet

In this section, a full wave digital model of the trumpet is presented. It is possible to estimate all geometrical bore parameters from acoustic measurements on a real instrument. Figure 8 shows the internal bore profile of a Boosey & Hawkes trumpet, as reconstructed from acoustic pulse reflectometry data using the layer-peeling method [16]. As can be seen from the bore profile, the main bore is essentially cylindrical, with an initial taper widening. This initial tapered section, which is usually referred to as the *lead-pipe*, is approximately conical. With the mouthpiece inserted, this part communicates with the backbore of the mouthpiece. Thus, an accurate model of the trumpet can be derived by approximating the bore profile data with a cylindrical bore, plus a conical section to model the lead-pipe, and modeling the remaining part of the reconstruction as the bell reflectance $R_L(\omega)$. What remains is (1) to model the mouthpiece, and (2) to formulate a suitable digital filter approximation of the bell reflectance.

4.1 Wave Digital Brass Mouthpiece Model

In the low-frequency limit, a small volume acts as a shunt compliance $C = V/(\rho c^2)$ [7]. Hence we suggest a mouthpiece model, in which the cup volume is modelled as a lumped element (a pure compliance), and the backbore is modelled as a distributed element (a conical section). Figure 9(a) shows the equivalent network of this arrangement. This model has been shown to be in good agreement with impedance measurements of brass instruments [30, 16], and is more suited to sound synthesis application than the "cylinder-cone model" suggested in [10], which causes spurious extra "multiplier regions" in the higher frequency range [16]. The mouthpiece model can be simulated in discrete-time by employing wave digital modeling techniques. The final "wave digital brass mouthpiece model" takes the form depicted in Figure 9(b). In a full instrument model (one that includes lip excitation), the left port of the system communicates directly with the unit that computes the non-linear flow through the lips. Because the lips will have an instantaneous reflection, the "cup volume unit" will have to have a zero instantaneous reflection towards the left, which can be realized by choosing the appropriate value for the port-resistance on that side of the unit. This results in using a WD-l volume structure, as shown in Figure 9c. The conical backbore can be modelled in the usual way. The WD-l volume unit has a non-zero instantaneous reflection towards the right, thus in order to avoid a delay-free loop, the left junction of the conical section needs to be modelled as a WD-l junction. The other junction (between the backbore and the lead-pipe) must be modelled with a normal WD junction, as described in Section 3.

For determination of the values of the port-resistances of each unit in Figure 9(b), one has to work from right to left, since the values of the distributed elements (R_3, R_4, R_5) must equal the local characteristic impedance. The values of R_1 and R_2 are arbitrary from a physical point of view but must be set to a specific value in order to ensure the realizability of the system. Applying the appropriate steps for deriving a wave digital model

of the shunt compliance part of the equivalent network in Figure 9(a) yields the WD-l volume is depicted in Figure 10 [16], where the values of the junction multiplier and the port-resistances are

$$k_j = -\frac{\beta C R_2}{1+\beta C R_2}, \quad R_2 = \frac{\beta M_1 R_3}{R_3+\beta M_1}, \quad R_1 = \frac{R_2}{1+\beta C R_2}, \tag{20}$$

where M_1 is the junction inertance associated with the WD-l junction.

4.2 The Bell Reflectance Filter

A brass bell functions as a reflector of waves, trapping energy inside the instrument in such a way that standing waves of precisely defined frequencies can be build up [31]. Since the bell has a fixed, time-invariant reflectance, it may be modelled as a lumped reflectance filter. A typical brass bell reflectance can be divided up in two stages: a slowly, quasi-exponentially rising build-up followed by a more oscillatory decay. The latter is generally readily approximated digitally by means of an IIR filter. However the first, rising part is something that classic IIR design techniques, such as output-error methods, generally tend to have problems with [32]. The simplest alternative is therefore to model the rising part as an FIR filter. The complete filter model then consists of an N-tap FIR in parallel to an IIR filter that is delayed by N samples. This approach is still considerably more efficient than using a single FIR filter. A very efficient alternative is to use truncated infinite impulse response (TIIR) filter elements to model the exponentially rising part [32]. With TIIR filters, one may implement exponentially rising responses using unstable one-pole elements; the filter stability can be guaranteed by using a "switched" version of the TIIR filter [33, 32]. A typical brass bell reflectance build-up only requires two first-order TIIR elements.

The complete wave digital model of the trumpet then takes the form depicted in Figure 11. In our implementation, fourth-order IIR filters were used for approximation of viscothermal losses in the main bore, and fractional delays were simulated by means of third-order Lagrange interpolators. A wave digital model is not stable if viscothermal losses are included in the conical sections (i.e., the lead-pipe and the backbore). Therefore this model has to be implemented in "switched" form, using two instances that run in parallel, as explained in Section 3.3. Figure 12(a) shows the Green's function (or impulse response) of the trumpet bore, as calculated with the transmission-line model and with the WDM method. The effects of simplifications and discretization are clearly extremely small in the first 35 ms of the response. More deviations occur in the latter part of the Green's function, which mainly has an effect on the lower frequency range. This can be observed in the comparison between the input impedances (the Fourier transforms of the respective Green's Functions) plotted in Figure 12(b). The WDM deviates from the ideal response particularly at the lowest resonance of the trumpet, mainly due to very small differences between the theoretical viscothermal losses and the digital approximation thereof. Fortunately, this discrepancy is not of that much relevance to musical sound synthesis,

as the lowest resonance of a trumpet is actually out of tune anyway and very seldom used as a fundamental in musical practice.

Sound output can be modelled using a transmittance filter $T_L(z)$ as schematically depicted in Figure 11. The power-response of this filter is complementary to that of the reflectance filter. The sound pressure p_{rad}, as obtained as the output of the transmittance filter, forms a first approximation to the radiated sound as would be heard by a listener, where we may expect that low-frequency components are more accurately modelled than high-frequency components, due to various simplifications used in the derivation of the wave digital model.

In a trumpet, the effective length of the bore is controlled by the player through valves. It would be straightforward to add this to the wave digital model, by modeling all tubular sections of a real trumpet, and inserting valve junctions that simply implement the appropriate amplitude weighting of tube input and output waves. Another, simpler approach would be to only adapt the length of the main cylindrical bore.

Finally, a realistic brass synthesis model requires the simulation of the effects of non-linear wave propagation, which causes the typical 'brassy' sound [34]. An efficient and robust method to achieve this was developed by Vergez and Rodet [35]; it can be directly applied within a wave-based modeling approach, and has already been built into "BRASS", the commercial brass synthesis software developed recently by IRCAM and Arturia [36].

5 Summary

Vibrations in musical wind instrument resonators can be efficiently synthesized digitally using wave-based methods, that explicitly simulate the transmission and reflectance of 1D waves in the instrument. Maintaining a spatially modular structure allows direct control of the musically important bore parameters such slide length or tonehole state. Unlike with the method of convolution with the full bore impulse response method, any change in such a parameters does not require the whole of this response to be re-calculated, but instead only a local parameter and it associated filter functions are changed. As such, modular wave-based methods are particularly suited to sound synthesis applications, in which the way in which parameters can be controlled is a crucial criterion [37].

Within the domain of modular wave-based approaches, the wave digital modeling (WDM) method provides a solid framework for deriving algorithmic modules for all relevant parts of wind instrument bores, including cylindrical and conical sections, mouthpieces, and flaring bells. In this approach, distributed elements are discretized using digital waveguide modeling techniques, and lumped elements are discretized using wave digital filter techniques. One of the key advantages of the WDM method is that delay-free loops can always be avoided without having to resort to simplifications or inserting artificial delays. It therefore allows accurate implementations at relatively low sample rates (e.g., 44.1 or 22.05 kHz) that can be run in real-time. The

WDM method requires considerably less computations than the multiconvolution algorithm and Ducasse's approach, that are both based on calculating all reflectances and transmittances via convolution. Although instability problems arise with bore models that include conical sections with loss-filters, a stable implementation is possible by using two switching instances of the same WDM bore model. A wave digital model of a complete trumpet bore was presented, which closely approximates all the important resonance qualities of the instrument. As shown in [25], the WDM can also be applied to synthesis of woodwind oscillations, including dynamical control of tonehole states. Future research in this area will include investigating whether instability problems associated with conical bore sections can be more directly addressed by preserving consistency in the use of the propagation constant; in the current formulations, the junctions are formulated using a lossless version of the propagation constant, which is a possible cause of instability problems [16]. Other issues that need further investigation are (1) the numerical artifacts that can occur when dynamically updating tonehole states, and (2) a better formulation of a resistive tonehole model, which would pave the way for improving the sound output with woodwind instruments.

References

[1] R. T. Schumacher. Self-sustained oscillations of the clarinet: An Integral Equation Approach. *Acustica*, 40:298–309, 1978.

[2] R. T. Schumacher. *Ab Initio* calculations of the oscillations of a clarinet. *Acustica*, 48(2):71–85, 1981.

[3] M. E. McIntyre, R. T. Schumacher, and J. Woodhouse. On the oscillations of musical instruments. *J. of the Acoust. Soc. of Am.*, 74(5):1325–1345, 1983.

[4] L. Hiller and P. Ruiz. Synthesizing musical sounds by solving thew ave equation for vibrating objects. *Journal of the Audio Engineering Society*, 19(6):462–470, 1971.

[5] S. Adachi and M. Sato. Time-domain simulation of sound production in the brass instrument. *J. of the Acoust. Soc. of Am.*, 97(6):3850–3861, 1995.

[6] B. Gazengel, J. Gilbert, and N. Amir. Time domain simulation of single reed wind instrument. From the measured input impedance to the synthesis signal. Where are the traps? *Acta Acustica*, 3:445–472, 1995.

[7] N. H. Fletcher and T. D Rossing. *The Physics of Musical Instruments*. Springer-Verlag, New York, 1991. Second Edition: 1998.

[8] D. H. Keefe. Physical modeling of wind instruments. *Computer Music J.*, 16:57–73, 1992.

[9] D.M. Campbell. Nonlinear dynamics of musical reed and brass wind instruments. *Contemporary Physics*, 40:415–431, 1999.

[10] R. Msallam, S. Dequidt, R. Caussé, and S. Tassart. Physical model of the trombone including nonlinear effects. Application to the sound synthesis of loud tones. *Acta Acustica*, 86(4):725–736, 2000. Special Issue on Musical Wind Instrument Acoustics.

[11] F. Avanzini. On the use of weighted sample methods in digitizing the clarinet equations. In *Proc. 2000 Int. Computer Music Conf.*, pages 46–49, Berlin, Germany, 2000. Computer Music Association.

[12] C. Vergez and X. Rodet. New algorithm for nonlinear propagation of a sound wave, application to a physical model of a trumpet. *Journal of Signal Processing*, 4(4):79–87, 2000.

[13] J. O. Smith. Physical modeling using digital waveguides. *Computer Music J.*, 16(4):74–91, 1992. Special issue: Physical Modeling of Musical Instruments, Part I.

[14] T. I. Laakso, V. Välimäki, M. Karjalainen, and M. Karjalainen. Splitting the unit delay – Tools for fractional delay filter design. *IEEE Signal Processing Magazine*, 13(1):30–60, 1996.

[15] V. Välimäki, M. Karjalainen, and T. I. Laakso. Modeling of woodwind bores with finger holes. In *Proc. 1993 Int. Computer Music Conf.*, pages 32–39, Tokyo, Japan, 1993. Computer Music Association.

[16] M. O. van Walstijn. *Discrete-Time Modelling of Brass and Reed Woodwind Instruments with Application to Musical Sound Synthesis*. PhD thesis, Faculty of Music, University of Edinburgh, 2002. http://www.ph.ed.ac.uk/∼maarten/.

[17] J. Abel, T. Smyth, and J.O. Smith. A simple, accurate wall loss filter for acoustic tubes. In *Proc. of the 6th International Conference on Digital Audio Effects (DAFx-03), London, UK*, London, 2003.

[18] H. Levine and J. Schwinger. On the radiation of sound from an unflanged circular pipe. *Phys. Rev.*, 73(4):383–406, 1948.

[19] G. P. Scavone. *An Acoustic Analysis of Single-Reed Woodwind Instruments with an Emphasis on Design and Performance Issues and Digital Waveguide Modeling Techniques*. PhD thesis, Music Dept., Stanford University, 1997. http://www.music.mcgill.ca/∼gary/thesis.html.

[20] V. Välimäki and M. Karjalainen. Digital waveguide modeling of wind instrument bores constructed of truncated cones. In *Proc. 1994 Int. Computer Music Conf.*, pages 423–430, Århus, Denmark, 1994. Computer Music Association.

[21] N. Amir, U. Shimony, and G. Rosenhouse. Discrete model for tubular acoustic systems with varying cross section - the direct and inverse problems. Part I: Theory. *Acta Acustica*, 81:450–462, 1995.

[22] J. Martínez, J. Agulló, and S. Cardona. Conical bores. Part II: Multiconvolution. *J. of the Acoust. Soc. of Am.*, 84(5):1620–1627, 1988.

[23] J. Gilbert, J. Kergomard, and J. D. Polack. On the reflection functions associated with discontinuities in conical bores. *J. of the Acoust. Soc. of Am.*, 87(4):1773–1780, 1990.

[24] J. Agulló, A. Barjau, and J. Martínez. On the time-domain description of conical bores. *J. of the Acoust. Soc. of Am.*, 91(2):1099–1105, 1992.

[25] M. O. van Walstijn and D.M. Campbell. Discrete-time modelling of woodwind instrument bores using wave variables. *J. of the Acoust. Soc. of Am.*, 113:575–585, 2003.

[26] A. Fettweis. Wave digital filters: Theory and practice. In *Proceedings of the IEEE*, pages 270–327, 1986.

[27] A. Barjau, D. H. Keefe, and S. Cardona. Time-domain simulation of acoustical waveguides with arbitrarily spaced discontinuities. *J. of the Acoust. Soc. of Am.*, 105(5):1951–1964, 1999.

[28] E. Ducasse. A physical model of a single-reed wind instrument, including actions of the player. *Computer Music Journal*, 27(1):59–70, 2003.

[29] A. H. Benade. Equivalent circuits for conical waveguides. *J. of the Acoust. Soc. of Am.*, 83(5):1764–1769, 1988.

[30] X. Lurton. Etude analytique de l'impédance d'entrée des instruments à embouchure. *Acustica*, 49:142–151, 1981.

[31] A. H. Benade. *Fundamentals of Musical Acoustics*. Oxford University Press, New York, 1976.

[32] M. O. van Walstijn and J. O. Smith. Use of truncated infinite impulse response (TIIR) filters in implementing efficient digital waveguide models of flared horns and piecewise conical bores with unstable one-pole filter elements. In *Proc. 1998 Int. Symposium on Musical Acoustics*, pages 309–314, Leavenworth, Washington, 1998. The Acoustical Society of America.

[33] A. L. Wang and J. O. Smith. On fast FIR filters implemented as tail-canceling IIR filters. *IEEE Trans. Signal Processing*, 45(6):1415–1427, 1997.

[34] A. Hirschberg, G. Gilbert, R. Msallam, and A. P. J. Wijnands. Shock waves in trombones. *J. of the Acoust. Soc. of Am.*, 99:1754–1758, 1996.

[35] C. Vergez and X. Rodet. Air flow related improvements for basic physical models of brass instruments. In *Proc. 2000 Int. Computer Music Conf.*, pages 62–65, Berlin, Germany, 2000. Computer Music Association.

[36] BRASS. commercial software for physics-based synthesis of trumpet, saxophone, and trombones sounds., 2005. Developed by IRCAM and Asturia. tt http://www.arturia.com/en/brass/entrypg.php.

[37] D. A. Jaffe. Ten criteria for evaluating synthesis techniques. *Computer Music J.*, 19(1):76–87, 1995.

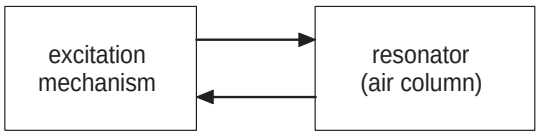

Figure 1: General structure of a physical model of a wind instrument. The air column functions as a passive resonating element that is 'blown' by the player via an excitation mechanism (for example a reed or the lips).

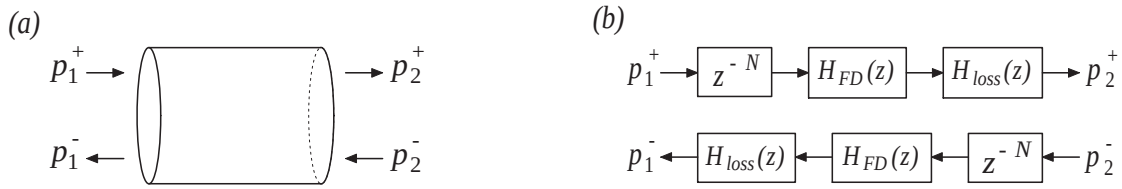

Figure 2: (a) Pressure waves at either side of a cylindrical duct section. (b) Digital waveguide model of lossy wave propagation in the cylindrical duct section. $H_{loss}(z)$ and $H_{FD}(z)$ denote a loss-filter and a fractional delay filter, respectively, and z^{-N} represents an N-sample long delay-line.

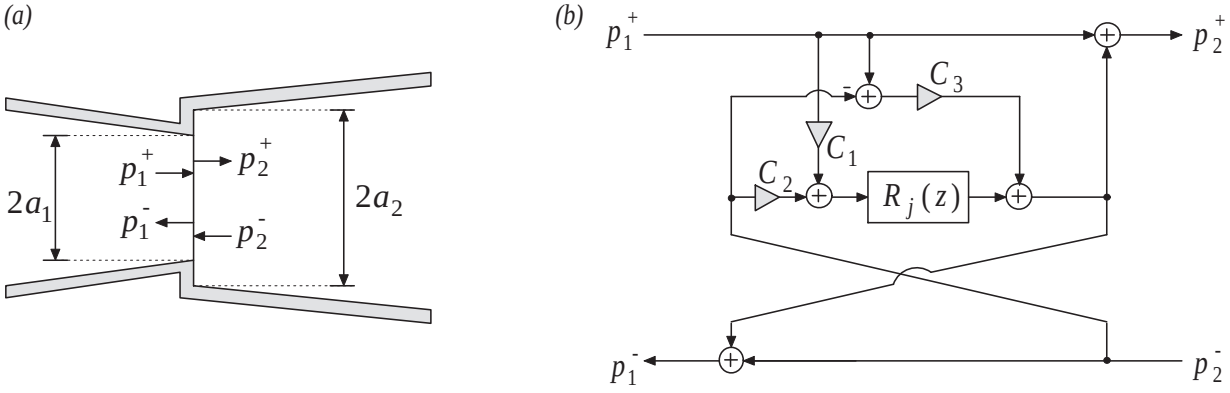

Figure 3: (a) A junction of two conical bore sections. (b) A digital waveguide junction in one-filter form.

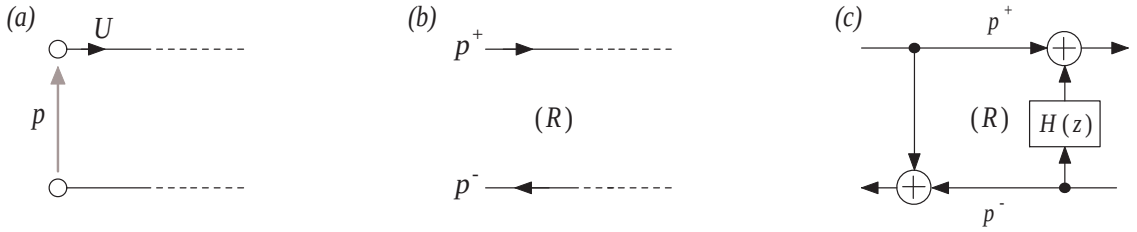

Figure 4: (a) A port and its associated acoustic variables. (b) The corresponding signal flow diagram after decomposition of the acoustic variables into wave variables. (c) A computational loop with transfer function $H(z)$ and port-resistance R.

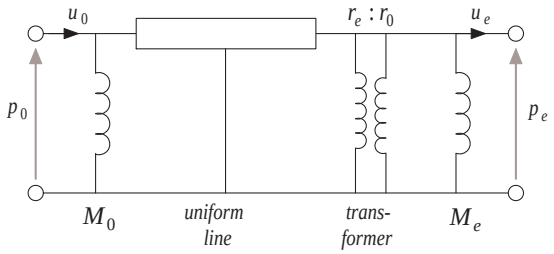

Figure 5: Equivalent circuit of a conical waveguide constructed of a uniform line, two shunt inertances, and transformer (after Benade [29]).

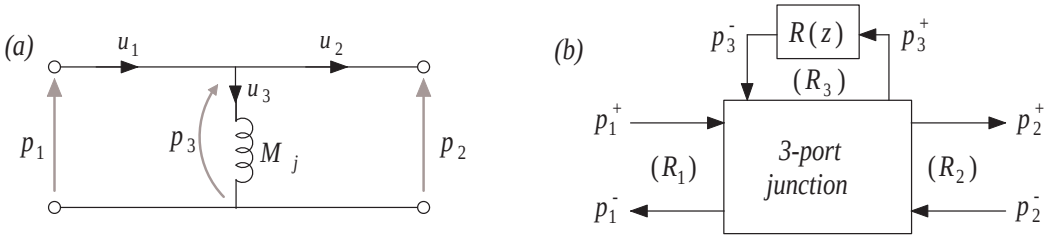

Figure 6: Wave digital modeling of a shunt junction inertance. (a) equivalent network. (b) Wave digital junction signal flow.

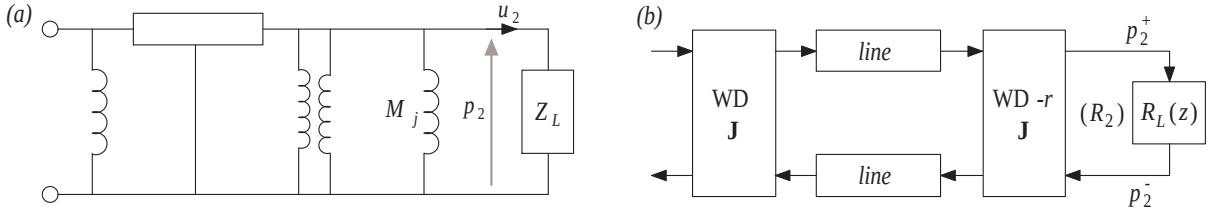

Figure 7: (a): The equivalent network of a conical junction that is terminated by an impedance load Z_L. (b): Signal flow diagram of a wave digital model. Each of the "*line*" units indicates a cascade of a digital delay-line, a fractional delay filter, and a loss-filter. The "WD **J**" unit represents a wave digital junction, and the "WD-r **J**" unit represents a wave digital junction with zero instantaneous reflection in right-going direction.

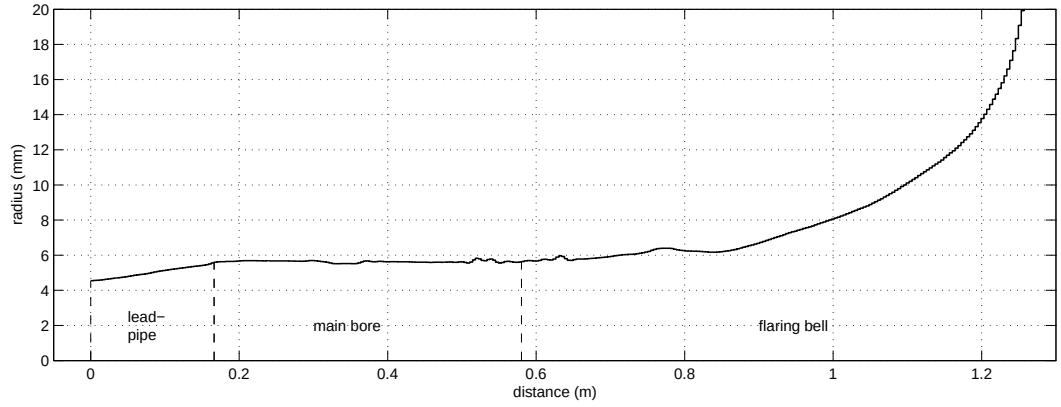

Figure 8: Trumpet bore profile reconstruction. The dashed lines indicate the division of the trumpet bore into a tapered section (the lead-pipe), a cylindrical section (the main bore), and a flared section (the bell).

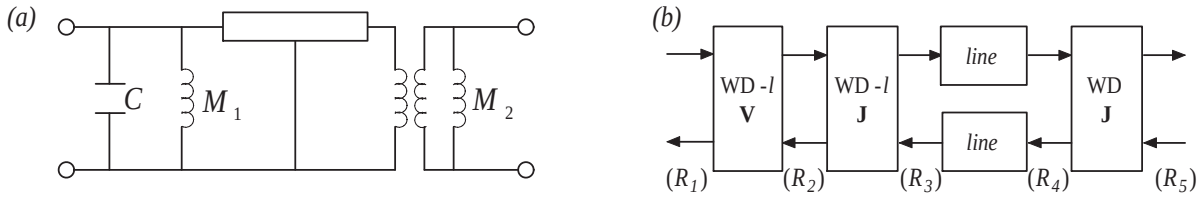

Figure 9: (a) Equivalent network of a brass mouthpiece. (b) Corresponding wave digital model. Each *line* unit indicates a cascade of delay-line, a fractional delay filter and a loss-filter. The WD-l **V** unit models the cup volume as a shunt compliance, and the WD-l **J** and WD **J** units model the junctions of the conical backbore with the cup volume and the lead-pipe, respectively. R_1, R_2, R_4, R_5, R_6 are the local port-resistances.

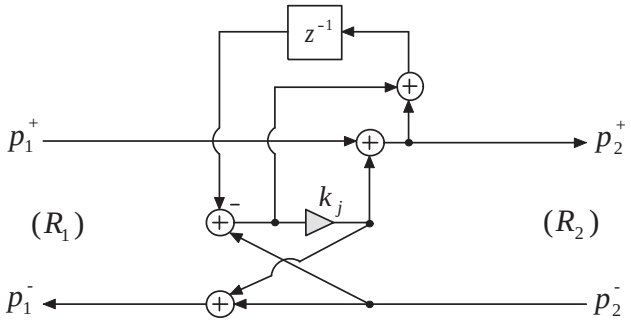

Figure 10: Signal flow of the WD-l volume.

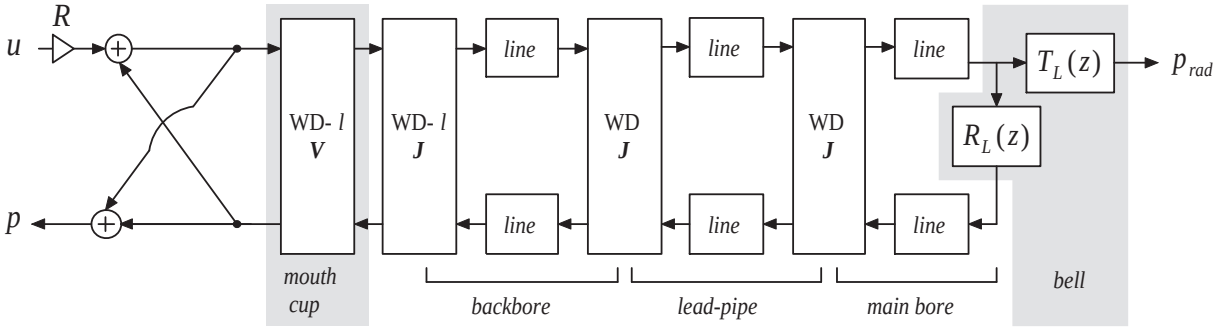

Figure 11: Wave digital model of the trumpet. The WD-l **V** unit indicates the wave digital volume structure that models the mouthpiece cup. The WD-l **J** unit indicates a wave digital junction that models the scattering of waves at the boundary between the mouthcup and the backbore. The WD **J** units indicate normal wave digital junctions, which model the taper and cross-sectional discontinuities at either end of the lead-pipe. The *line* units implement lossy wave propagation. R is the port-resistance at the input-end.

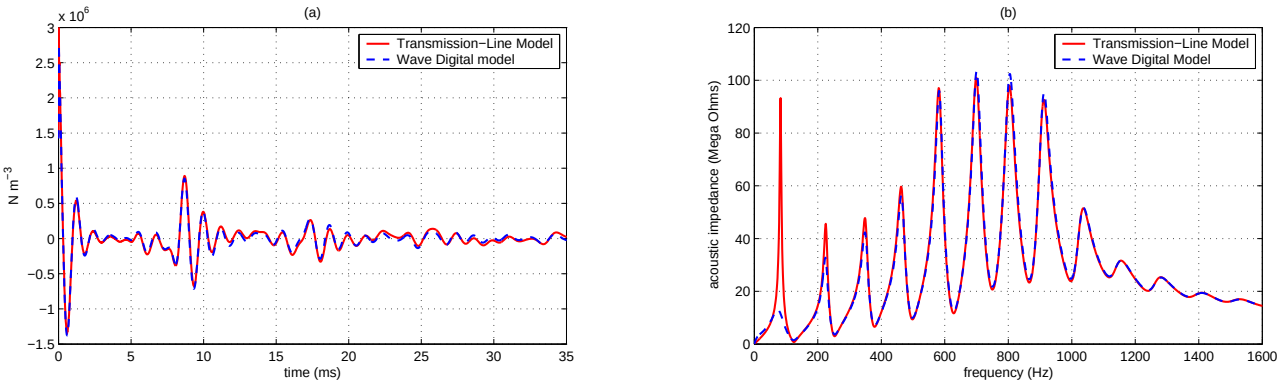

Figure 12: (a) Discrete-time Green's function of the Boosey and Hawkes trumpet bore. (b) Input impedance of the Boosey and Hawkes trumpet. The sample rate is 44.1 kHz.